

Antiferromagnetic MnO nanoparticles with ferrimagnetic Mn₃O₄ shells: Doubly inverted core-shell system

A. E. Berkowitz,^{1,2} G. F. Rodriguez,¹ J. I. Hong,² K. An,³ T. Hyeon,³ N. Agarwal,⁴ D. J. Smith,⁴ and E. E. Fullerton^{2,5}

¹Department of Physics, University of California-San Diego, La Jolla, California 92093, USA

²Center for Magnetic Recording Research, University of California-San Diego, La Jolla, California 92093, USA

³National Creative Research Initiative Center for Oxide Nanocrystalline Materials, Seoul National University, Seoul 151-744, Korea

⁴School of Materials and Department of Physics, Arizona State University, Tempe, Arizona 85287, USA

⁵Department of Electrical and Computer Engineering, University of California-San Diego, La Jolla, California 92093, USA

(Received 4 July 2007; revised manuscript received 25 October 2007; published 2 January 2008)

We report the magnetic and microstructural properties of antiferromagnetic MnO nanoparticles with shells of ferrimagnetic Mn₃O₄, which is opposite the usual arrangement of antiferromagnetically coated ferromagnetic nanoparticles. In addition, the antiferromagnetic MnO cores order at much higher temperature ($T_N=118$ K) than the ferrimagnetic Mn₃O₄ shells ($T_C=43$ K)—another reversal of the usual situation. The single crystal MnO cores, with rocksalt structure, are crystallographically aligned with the tetragonal spinel structure of the Mn₃O₄ shells. Particles field cooled in 50 kOe have large coercive force and exchange bias below T_C , e.g., 5800 and 2950 Oe, respectively, at 5 K. The spontaneous magnetization at $T_C(\text{Mn}_3\text{O}_4)$ is $\sim 20\%$ of its value at 5 K, and remains finite for more than 20 K above $T_C(\text{Mn}_3\text{O}_4)$. Hysteresis with exchange bias is present in this anomalous region. The MnO cores with their uncompensated spins are responsible for the behavior above $T_C(\text{Mn}_3\text{O}_4)$. The MnO cores have a blocking temperature of 95 K, and the hysteresis and exchange bias above $T_C(\text{Mn}_3\text{O}_4)$ results from the switching of the MnO spin lattices by their uncompensated spins. Analysis of the thermoremanent magnetization and field cooling and/or zero field cooling in 50 kOe, and the dependence of exchange bias on the temperature at which the cooling field was applied support this model.

DOI: [10.1103/PhysRevB.77.024403](https://doi.org/10.1103/PhysRevB.77.024403)

PACS number(s): 75.75.+a, 68.35.Ct, 68.37.Lp

I. INTRODUCTION

Meiklejohn and Bean discovered exchange anisotropy in nanoparticles (NP's) consisting of a ferromagnetic (FM) Co core and an antiferromagnetic (AF) CoO shell, with the magnetic ordering temperatures $T_C(\text{Co}) > T_N(\text{CoO})$.¹ For more than 50 years since that discovery, investigations of exchange anisotropy in NP have generally involved systems following the Meiklejohn-Bean paradigm, namely, FM core with AF shell and $T_C > T_N$, as discussed in the review by Nogués *et al.*² Since many transition metal oxides are AF (e.g., NiO, CoO, FeO, and $\alpha\text{-Fe}_2\text{O}_3$), and these are native oxides of the respective transition metals, most core-shell samples studied have been prepared by oxidizing the metal particles. Control of the size distribution and of the core and shell dimensions is generally difficult with these oxidized particles, and, quoting Ref. 2, “another drawback is that, due to the shape of the nanoparticles and their reduced size, the AFM shell usually grows highly disordered, making the control of its microstructure rather difficult.” For these reasons, our basic understanding of exchange anisotropy in core-shell systems is much less advanced than is the case for FM-AF binary film systems.

We report here the behavior of core-shell NP in which not only are both features of the Meiklejohn-Bean paradigm inverted, but the core and shell microstructures are very well defined, and the size distribution is narrow. These NP's consist of AF MnO cores with ferrimagnetic Mn₃O₄ shells; and $T_N(\text{MnO})$ is 118 K,³ whereas $T_C(\text{Mn}_3\text{O}_4)$ is only 43 K.⁴ The single crystal MnO cores with rocksalt structure are crystallographically aligned with the tetragonally deformed spinel

Mn₃O₄. A microstructural model is developed which accounts for the alignment of these two dissimilar structures. Very large coercive force (H_C), i.e., half the sum of the absolute values of the two fields at which the magnetization is zero, and exchange bias (H_E), i.e., hysteresis loop shifts along the applied field axis, appear at low temperatures for field-cooled samples. At $T_C(\text{Mn}_3\text{O}_4)$, the spontaneous magnetization declines sharply but retains $\sim 20\%$ of its magnitude at 5 K, and does not vanish until much higher temperatures. Hysteresis loops at temperatures within this anomalous region exhibit finite H_C and H_E . The thermoremanent magnetization (TRM) is likewise finite at temperatures well above $T_C(\text{Mn}_3\text{O}_4)$. These anomalous properties are due to uncompensated spin moments on the MnO-NP surfaces, with the hysteresis arising from the switching of the magnetic sublattices of the MnO NP by the torque exerted by uncompensated spins. The uncompensated spins are also responsible for establishing H_E in these NP with T_N greater than T_C —on field cooling the frozen polarized MnO uncompensated spins polarize the Mn₃O₄ by exchange coupling below T_C . The MnO-NP exhibit a blocking temperature (T_B) ~ 20 K below T_N .

Several previous investigations of nominal MnO NP have observed the magnetization to decline at ~ 43 K and attributed this to finite size reductions of the bulk $T_N(\text{MnO})$.⁵⁻¹⁰ Another study of oxidized Mn NP inferred an inverted behavior associated with the presence of MnO and Mn₃O₄.¹¹ In the present study, microstructural and magnetic data confirm unambiguously the existence of NP with MnO cores and Mn₃O₄ shells.

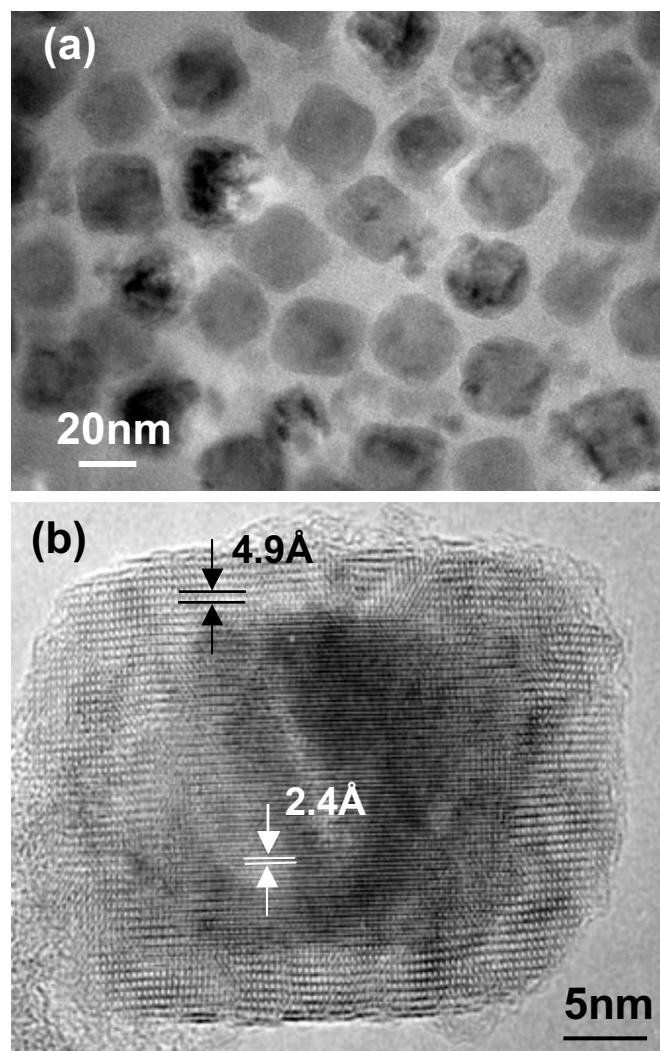


FIG. 1. (a) Low resolution electron micrograph showing array of MnO/Mn₃O₄ NP supported on thin carbon film. (b) High resolution electron micrograph of MnO/Mn₃O₄ NP showing alignment of the (111) lattice planes of both phases.

II. SAMPLE PREPARATION AND STRUCTURAL CHARACTERIZATION

The MnO/Mn₃O₄ NP were prepared by thermal decomposition of a Mn-oleate complex in a high boiling point organic solvent.¹² The as-prepared particles with excess oleic acid were stored in hexane. The nominal objective was to prepare MnO-NP. It is not clear whether the Mn₃O₄ shell was present in the initial preparation, or whether it evolved during storage. However, over the time scale of our measurements, the particle structures did not change. The particles were washed in combinations of methanol, acetone, and hexane until they were free of excess oleic acid (clear solution, particles readily precipitated). Samples of as-prepared and washed particles were dried and mounted for superconducting quantum interference device (SQUID) measurements in Ag cups, which were pressed into disks to immobilize and protect the particles.

Figure 1(a) is a low magnification electron micrograph of an array of the as-prepared MnO/Mn₃O₄ NP. The NP's have

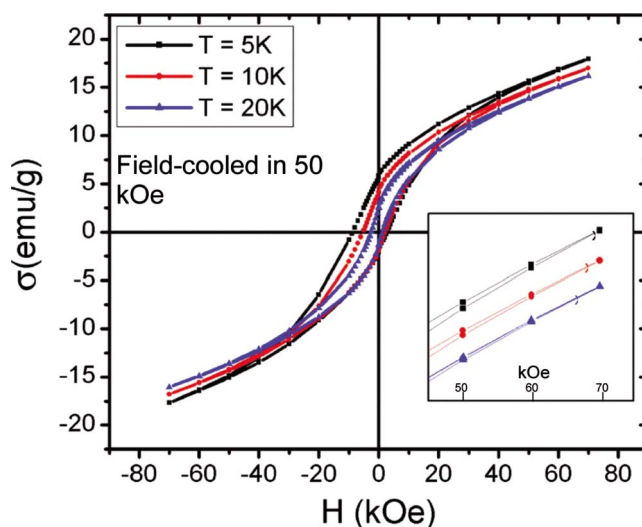


FIG. 2. (Color online) Hysteresis loops of the MnO/Mn₃O₄ NP at indicated temperatures. Inset shows increasing bifurcation field with decreasing temperature.

rhomboidal shapes with average sizes of 26–28 nm. Details of a single particle are shown at higher magnification in Fig. 1(b). The [111] lattice images of the core and the surrounding shell are clearly visible. The Mn₃O₄ shell has an average thickness of ~ 4 nm, and has the tetragonal hausmanite structure (tetragonally deformed from the high temperature cubic spinel form) with lattice parameters $a_{\text{spinel}} = 8.153 \text{ \AA}$ and $c = 1.16a_{\text{spinel}}$.¹³ The single crystal MnO core has the rocksalt structure with $a = 4.445 \text{ \AA}$.³ Despite the mismatch between the crystal structures and the lattice spacings, the core and shell are crystallographically well aligned. The NP's exhibited broad and shallow x-ray diffraction peaks at the [211], [103], and [220] Mn₃O₄ positions, and broad electron diffraction rings with diameters consistent with the large Mn₃O₄ unit cell.

III. MAGNETIC PROPERTIES

Hysteresis loops measured below $T_C(\text{Mn}_3\text{O}_4)$ after field cooling in 50 kOe are shown in Fig. 2. The characteristic high field susceptibility found in bulk¹⁴ and NP Mn₃O₄ (Ref. 15) is evident. Mn₃O₄ has a normal spinel spin occupancy with the Mn³⁺ cations in the octahedral B sites and the Mn²⁺ cations in the tetrahedral A sites. The Mn³⁺ spins are not collinear, but are canted with a net moment antiparallel to the Mn²⁺ spins. The high field susceptibility results from rotation of the canted spins into the field direction. In the inset in Fig. 2, the high field region is expanded. As the temperature is decreased, the bifurcation field increases until it reaches the maximum measuring field of 70 kOe at 5 K. The bifurcation field is the maximum field at which irreversible switching of the magnetization occurs. These high switching fields are consistent with the reported anisotropy field of 74 kOe at 4.2 K along the hard c axis.¹⁶

The spontaneous magnetization σ_0 was determined by extrapolating the high field magnetization back to $H=0$.

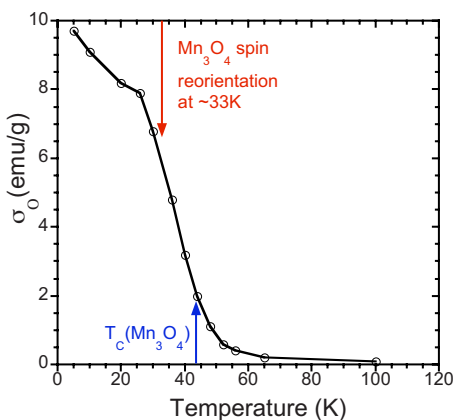


FIG. 3. (Color online) Temperature dependence of spontaneous magnetization of MnO/Mn₃O₄ NP.

Its temperature dependence is shown in Fig. 3. The slope changes in the region where a commensurate/incommensurate spin transition occurs,¹⁷ and an inflection point is present near $T_C(\text{Mn}_3\text{O}_4)$. σ_0 reduces sharply near $T_C(\text{Mn}_3\text{O}_4)$, but, remarkably, at $T_C(\text{Mn}_3\text{O}_4)$ it retains the high value of 20% of $\sigma_0(5\text{ K})$ and does not vanish until $>65\text{ K}$.

The temperature dependence of H_E and H_C after field cooling from 300 to 5 K in 50 kOe [field cooled (FC)], and for 5, 10, and 20 K in 0 kOe [zero field cooled (ZFC)], are plotted in Fig. 4. The large H_C at low temperatures arises from the switching of single domain Mn₃O₄ NP with their large magnetocrystalline anisotropy. The FC- H_C has a minimum in the region of the spin reorientation, but remains measurable until $>65\text{ K}$. The smaller ZFC- H_C is due to the random alignments of both the magnetocrystalline anisotropy axes and the contributions of exchange anisotropy for that case. ZFC- H_E is vanishingly small as a result of the almost completely random distribution of the NP interfaces—its finite value demonstrates the difficulty of achieving a perfectly random distribution. As with σ_0 and H_C , the FC- H_E remains measurable until $>65\text{ K}$.

Mn₃O₄ is a native oxide of MnO, as reported for bulk¹⁸ and NP¹⁹ samples. The interfacial microstructure must be

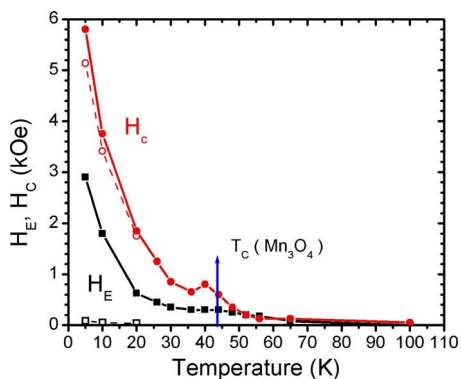


FIG. 4. (Color online) Temperature dependence of H_E and H_C . Solid points after field cooling in 50 kOe; hollow points after zero-field cooling.

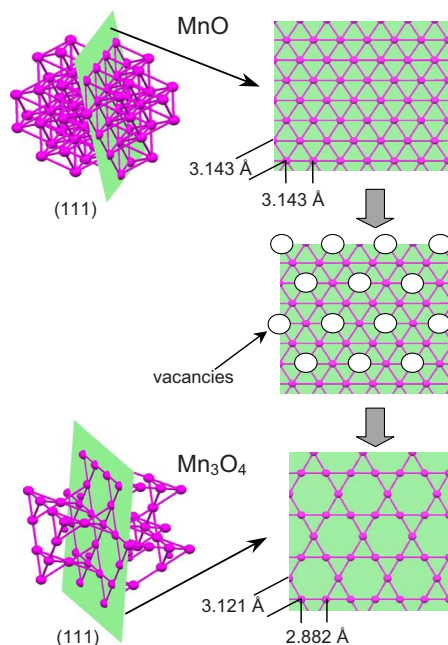


FIG. 5. (Color online) Schematic showing Mn atoms in MnO and Mn₃O₄ lattices and their arrangements on the respective (111) planes.

consistent with the alignment of the core and shell lattice planes. A model applicable to the growth of Mn₃O₄ on MnO has been discussed by Catlow and Fender²⁰ for the similar structural consideration of Fe₃O₄ impurities in Fe_(1-X)O. The model follows from the facts that the usual defect present in MnO is a Mn²⁺ vacancy which can be compensated by the formation of Mn³⁺ ions, and that the lowest energy distributions of the Mn²⁺ vacancies and Mn³⁺ ions favor the formation of clusters consisting of four octahedral vacancies surrounding a tetrahedrally coordinated Mn³⁺. These clusters energetically tend to aggregate by edge and corner sharing, and one such aggregate is an element of the spinel structure from which Mn₃O₄ can develop. Figure 5 shows schematically how Mn²⁺ vacancies on the MnO (111) plane produce an atomic coordination similar to the (111) plane of Mn₃O₄.²¹ The cluster aggregate model implies the presence of Mn³⁺ ions with $4\mu_B$ spins on the surfaces of the MnO-NP. If these spins are uncompensated or ordered, as well as Mn²⁺ uncompensated spins due to the vacancies and to the usual finite size effects, plus the likelihood of polarization of some interfacial Mn₃O₄ by virtue of proximity to the ordered MnO, the combination would account for the significant value of σ_0 above $T_C(\text{Mn}_3\text{O}_4)$.

Support for such a model comes from the TRM in Fig. 6, which shows the temperature dependence of the TRM, normalized to the values at 10 K, for as-prepared and washed samples after field cooling in 50 kOe to 10 K and then measuring the remanent moment in zero field. As seen in Fig. 6(a), Mn₃O₄ dominates the TRM below its T_C . Above 43 K [Fig. 6(b)], the TRM is the moment of the frozen polarized uncompensated spins on the surfaces of the MnO-NP. As shown in the inset of Fig. 6, the normalized TRM indicates that the blocking temperature of the MnO-NP is 95 K. To

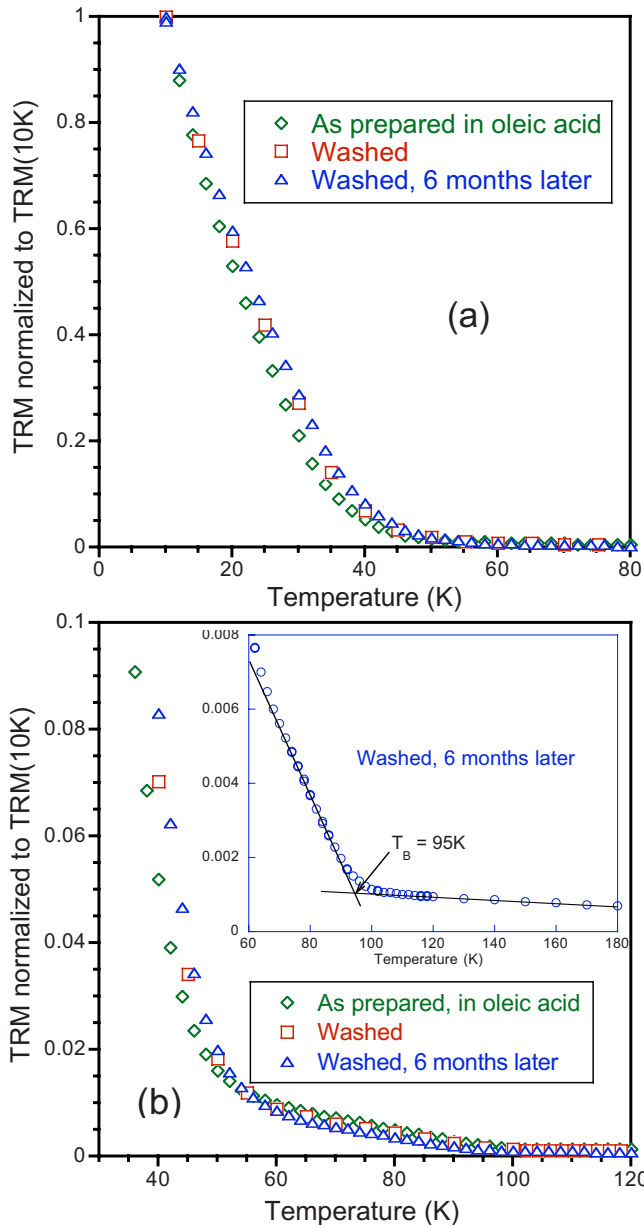


FIG. 6. (Color online) TRM normalized to the value at 10 K. Shown are data for the as-prepared sample and two measurements of the washed sample. (a) and (b) show data for low and high temperatures, respectively. The inset in (b) shows the expanded high temperature data which permits the identification of T_B .

justify this conclusion, the MnO cores in the NP can be approximated as cubes with 20 nm edges. For SQUID measurements that take about a minute per point, it is generally agreed that KV/kT , where K is the anisotropy constant of NP with volume V , should be about 25 for thermal stability. Bloch *et al.*²² have estimated from susceptibility measurements that the weak (111) plane anisotropy $K_2=9 \times 10^3$ erg/cc at 4.2 K. This makes $K_2V/kT=120$ at 4.2 K. With K_2 remaining constant, K_2V/kT would be 5 at 95 K. Since K_2 is generally smaller at 95 K than at 4.2 K, it is quite reasonable to take 95 K as the blocking temperature T_B of the MnO-NP, where T_B is the temperature at which the large-

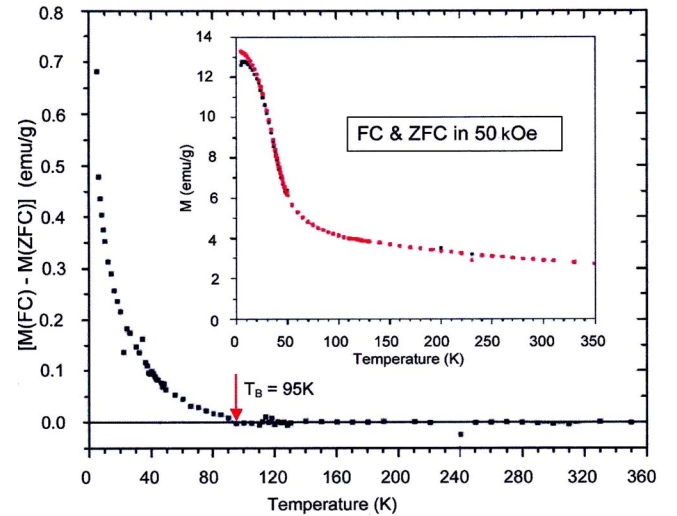


FIG. 7. (Color online) FC and ZFC magnetization in 50 kOe. The inset shows the FC (red) and ZFC (black) curves. The main curve shows (FC-ZFC), which vanishes at 95 K.

est MnO particles become superparamagnetic. The temperature dependence of the TRM above 43 K is similar to that of other monoxides such as CoO (Ref. 23) and $\text{Co}_{0.52}\text{Ni}_{0.48}\text{O}$,²⁴ namely, relatively flat at high temperatures, with a sharp increase at lower temperatures. The increase at low temperatures is likely due to a high density of uncompensated spins that are more weakly exchange coupled to the MnO-NP.

FC and ZFC magnetization measurements were made in several fields as functions of temperature. Measurements at 10 and 100 Oe reflected principally the complex field-dependent switching of the Mn_3O_4 NP, and did not provide particularly useful insight into basic NP properties. However, the 50 kOe runs, shown in Fig. 7, were very helpful in corroborating the value of T_B . FC/ZFC runs in 50 kOe are close to a “ground state” in that the FC alignment is virtually complete, and we may regard the ZFC values as truly reversible. Therefore, the difference between them is a measure of irreversibility. In Fig. 7, (FC-ZFC) vanishes at 95 K, precisely the value of T_B derived from the TRM, as shown in Fig. 6. The irreversibility measured by the 50 kOe runs above 43 K consists of the switching of MnO NP by their uncompensated spins, as previously discussed. Thus, when the most stable MnO NP becomes superparamagnetic, irreversibility vanishes, and that temperature is T_B .

The properties of the NP above $T_C(\text{Mn}_3\text{O}_4)$ originate from the following microstructural and/or magnetic considerations: The crystallographic alignment of the ~ 4 nm Mn_3O_4 shells with the ~ 20 nm MnO cores implies the presence of Mn^{3+} ($4\mu_B$) defects on the MnO interfacial surfaces, as well as the defects associated with the vacancies present. These defects contribute to the MnO uncompensated spin moment at temperatures above $T_C(\text{Mn}_3\text{O}_4)$ in addition to the uncompensated spins arising from finite size effects, producing a seemingly anomalous σ_0 . The finite values of H_C and H_E of field-cooled NP are due to the switching of the MnO-NP spin systems by the biased uncompensated spins to which they are exchange coupled. This switching is facilitated at these elevated temperatures by the low anisotropy of MnO, and by

TABLE I. H_E and H_C after indicated field-cooling protocols.

ZFC from 350 K to (X) K, then FC in 5 T to 10 K. X (K)	FC from 350 K in 5 T to (Y) K, then ZFC to 10 K. (Y) K	H_E at 10 K (Oe)	H_C at 10 K (Oe)
	10	1884	4384
70		1871	4371
	70	471	4082
50		1554	4286
40		1415	4335
30		1096	4292
10		71	3905
	10 (1 month later)	1867	4349

thermally activated reduction of energy barriers, as indicated by the fact that T_B is ~ 23 K less than $T_N(\text{MnO})$.

Another series of experiments provided additional information about the NP model and the general issue of how H_E is established when T_N is considerably greater than T_C . Various FC protocols were applied, with the results shown in Table I. H_E and H_C were measured at 10 K after (a) zero field cooling to the indicated temperatures in the first column and field cooling in 5 T to 10 K, and (b) field cooling in 5 T to the indicated temperatures in the second column and then zero field cooling to 10 K. The most significant results of these experiments are the following:

(i) Field cooling to 70 K, then zero field cooling to 10 K produce 25% of maximum H_E . This result shows that uncompensated spins on MnO-NP with the highest energy barriers are pinned by field cooling to 70 K, and that these spins, in turn, bias the Mn_3O_4 to which they are exchange coupled as the Mn_3O_4 magnetically orders on cooling in zero field below 43 K.

(ii) Zero field cooling to 70 K and then field cooling to 10 K yield the same H_E as the full field cooling to 10 K from 350 K. Evidently, the MnO anisotropy at 70 K, assisted by thermal activation, produces energy barriers low enough for the 5 T cooling field to polarize all MnO-NP in the field direction as effectively as when field cooled from 350 K.

(iii) Zero field cooling to $T \leq 50$ K and then field cooling to 10 K yield progressively lower H_E until H_E is negligible for zero field cooling to 10 K. An important feature of these data is that field cooling from 50 K, $> T_C(\text{Mn}_3\text{O}_4)$, does not produce maximum H_E as does field cooling from 70 K. If the polarization of paramagnetic Mn_3O_4 was responsible for H_E , then field cooling from both 70 and 50 K would be expected to yield maximum H_E at 10 K since both temperatures are $> T_C(\text{Mn}_3\text{O}_4)$.

(iv) H_C is not strongly dependent on the field-cooling protocol—it is moderately reduced as spin alignment is reduced, i.e., as H_E decreases.

IV. CONCLUSIONS

In addition to inverting the usual FM-AF core-shell structures and magnetic ordering temperatures, the MnO/ Mn_3O_4 NP impact a variety of issues; namely, the growth of native oxides on monoxide AF-NP; how exchange anisotropy is established in doubly inverted NP; the role of AF uncompensated spins in the hysteresis of AF-NP; the origin of the magnetic properties of the FM-AF interface; and the basic properties that define the blocking temperatures of AF-NP. The alignment of the MnO core and Mn_3O_4 shell lattice planes shown in Fig. 1 strongly supports the atomic arrangement sketched in Fig. 5. Such an ordered interface, albeit with some Mn^{3+} defects, implies strong interfacial MnO/ Mn_3O_4 coupling. This is confirmed by the large H_E below $T_C(\text{Mn}_3\text{O}_4)$. The manner by which H_E is established in this system, where T_N is so much higher than T_C , is straightforward—as MnO is cooled in a field from above T_N , its uncompensated spins are frozen with a net polarization in the field direction. These polarized spins induce the same polarization direction in the Mn_3O_4 by exchange coupling as the NP's are cooled below $T_C(\text{Mn}_3\text{O}_4)$. As the cooling field is applied at progressively lower temperatures, H_E is reduced since more uncompensated spins have been frozen in random directions. The appearance of H_E and H_C above $T_C(\text{Mn}_3\text{O}_4)$ is a vivid demonstration of irreversible switching of AF spin lattices by exchange-coupled uncompensated spins—with the assistance of thermal activation. The TRM of the MnO-NP above $T_C(\text{Mn}_3\text{O}_4)$ has a similar temperature dependence to that observed in polycrystalline films of AF monoxides, i.e., a relatively flat higher temperature region with a sharp upswing at lower temperatures. It seems very reasonable to consider that the low temperature TRM upswing represents uncompensated spins more weakly coupled to the MnO cores e.g., either further away or with superexchange angles less than 180° . Finally, the behavior of the H_C , H_E , σ_0 , TRM, and FC-ZFC of the MnO-NP above $T_C(\text{Mn}_3\text{O}_4)$ provides an exhaustively characterized example of the properties of relatively monodispersed AF monoxide NP up to T_B . This latter feature is a direct consequence of the double inversion—FM on the AF surface with T_C less than T_N . Finally, it is possible that the conclusions reached in this investigation can explain some of the properties reported in previous studies of MnO-NP's.^{5–10,25}

ACKNOWLEDGMENTS

We deeply appreciate pertinent discussions of this investigation with I. S. Jacobs, F. T. Parker, F. S. Spada, and S. Seehra. We acknowledge use of facilities in the John M. Cowley Center for High Resolution Electron Microscopy at Arizona State University. Recently, the results of Ref. 25 came to our attention, which discussed the magnetic properties of a series of spheroidal particles ranging from the smallest Mn_3O_4 NP's to larger particles with MnO cores and Mn_3O_4 shells.

- ¹W. H. Meiklejohn and C. P. Bean, *Phys. Rev.* **102**, 1413 (1956).
- ²J. Nogués, J. Sort, V. Langlais, V. Skumryev, S. Suriñach, J. S. Muñoz, and M. D. Baró, *Phys. Rep.* **422**, 65 (2005).
- ³A. P. Kantor, L. S. Dubrovinsky, N. A. Dubrovinskaia, I. Y. Kantor, and I. N. Goncharenko, *J. Alloys Compd.* **402**, 42 (2005).
- ⁴R. A. Robie and B. S. Hemmingway, *J. Chem. Thermodyn.* **17**, 165 (1985).
- ⁵G. H. Lee, S. H. Huh, J. W. Jeong, B. J. Choi, S. H. Kim, and H.-C. Ri, *J. Am. Chem. Soc.* **124**, 12094 (2002).
- ⁶W. S. Seo, H. H. Jo, K. Lee, B. Kim, S. J. Oh, and J. T. Park, *Angew. Chem.* **116**, 1135 (2004).
- ⁷Y. Q. Chang, D. P. Yu, Z. Wang, Y. Long, H. Z. Zhang, and R. C. Ye, *J. Cryst. Growth* **281**, 678 (2005).
- ⁸O. Masala and R. Seshadri, *J. Am. Chem. Soc.* **127**, 9354 (2005).
- ⁹M. A. Morales, R. Skomski, S. Fritz, G. Shelburne, J. E. Shield, M. Yin, S. O'Brien, and D. L. Leslie-Pelecky, *Phys. Rev. B* **75**, 134423 (2007).
- ¹⁰M. Yin and S. O'Brien, *J. Am. Chem. Soc.* **125**, 10180 (2003). We note that in the Supporting Information for this paper, a selected area electron diffraction pattern shows broad diffuse inner rings which could be associated with the large unit cell of thin Mn_3O_4 .
- ¹¹P. Z. Si, D. Li, J. W. Lee, C. J. Choi, Z. D. Zhang, D. Y. Geng, and E. Brück, *Appl. Phys. Lett.* **87**, 133122 (2005).
- ¹²J. Park, K. An, Y. Hwang, J.-G. Park, H.-J. Noh, J.-Y. Kim, J.-H. Park, N.-M. Hwang, and T. Hyeon, *Nat. Mater.* **3**, 891 (2004).
- ¹³D. Jarosch, *Mineral. Petrol.* **37**, 15 (1987).
- ¹⁴I. S. Jacobs, *J. Phys. Chem. Solids* **11**, 1 (1959).
- ¹⁵E. Winkler, R. D. Zysler, and D. Fiorani, *Phys. Rev. B* **70**, 174406 (2004).
- ¹⁶O. V. Nielsen, *J. Phys. (Paris)* **32**, C1 (1971).
- ¹⁷G. B. Jensen and O. V. Nielsen, *J. Phys. C* **7**, 409 (1974).
- ¹⁸M. S. Jagadeesh and M. S. Seehra, *Phys. Rev. B* **21**, 2897 (1980).
- ¹⁹J. Park, E. Kang, C. J. Bae, J.-G. Park, H.-J. Noh, J.-Y. Kim, J.-H. Park, H. M. Park, and T. Hyeon, *J. Phys. Chem. B* **108**, 13594 (2004).
- ²⁰C. R. A. Catlow and B. E. F. Fender, *J. Phys. C* **8**, 3267 (1975); *J. Phys. (Paris), Colloq.* **C7**, 67 (1977).
- ²¹This is the (111) plane of Mn_3O_4 as derived from the cubic spinel structure with lattice parameters $a_{\text{tet}}=a_{\text{spinel}}$ and $c=1.16a_{\text{spinel}}$. Another description has $c=1.16a_{\text{spinel}}$ and $a'=a_{\text{spinel}}/\sqrt{2}$ along the (110) direction of the original spinel lattice.
- ²²D. Bloch, J. L. Feron, R. Georges, and I. S. Jacobs, *J. Appl. Phys.* **38**, 1474 (1967).
- ²³Kentaro Takano, R. H. Kodama, A. E. Berkowitz, W. Cao, and G. Thomas, *Phys. Rev. Lett.* **79**, 1130 (1997).
- ²⁴A. E. Berkowitz, M. F. Hansen, R. H. Kodama, Y. J. Tang, J. I. Hong, and David J. Smith, *Phys. Rev. B* **72**, 134428 (2005).
- ²⁵G. Salazar-Alvarez, J. Sort, S. Surinach, M. Dolores Baro, and Josep Nogués, *J. Am. Chem. Soc.* **129**, 9102 (2007).